

**OBGC in the warm  
climate of the Late  
Paleocene**

M. Heinze and T. Ilyina

# Ocean Biogeochemistry in the warm climate of the Late Paleocene

M. Heinze<sup>1,2</sup> and T. Ilyina<sup>1</sup>

<sup>1</sup>Max Planck Institute for Meteorology, Bundesstrasse 53, 20146 Hamburg, Germany

<sup>2</sup>International Max Planck Research School on Earth System Modelling, Hamburg, Germany

Received: 24 March 2014 – Accepted: 7 April 2014 – Published: 28 April 2014

Correspondence to: M. Heinze (mathias.heinze@mpimet.mpg.de)

Published by Copernicus Publications on behalf of the European Geosciences Union.

Title Page

Abstract

Introduction

Conclusions

References

Tables

Figures

⏪

⏩

◀

▶

Back

Close

Full Screen / Esc

Printer-friendly Version

Interactive Discussion



## Abstract

The Late Paleocene is characterized by warm and stable climatic conditions which served as the background climate for the Paleocene-Eocene Thermal Maximum (PETM, ~ 55 million years ago). With respect to feedback processes in the carbon cycle, the ocean biogeochemical background state is of major importance for projecting the climatic response to a carbon perturbation related to the PETM. Therefore we use the Hamburg Ocean Carbon Cycle model HAMOCC, embedded into the ocean general circulation model of the Max Planck Institute for Meteorology, MPIOM, to constrain the ocean biogeochemistry of the Late Paleocene. We focus on the evaluation of modeled spatial and vertical distributions of the ocean carbon cycle parameters in a long-term warm steady-state ocean, based on a 560 ppm CO<sub>2</sub> atmosphere. Model results are discussed in the context of available proxy data and simulations of pre-industrial conditions. Our results illustrate that ocean biogeochemistry is shaped by the warm and sluggish ocean state of the Late Paleocene, which affects the strength and spatial variation of the different carbon pumps. Primary production is only slightly reduced in comparison to present-day; it is intensified along the equator, especially in the Atlantic. This enhances remineralization of organic matter, resulting in strong oxygen minimum zones and CaCO<sub>3</sub> dissolution in intermediate waters. We show that an equilibrium CO<sub>2</sub> exchange without increasing total alkalinity concentrations above today's values is achieved. Yet, the surface ocean pH and the saturation state with respect to CaCO<sub>3</sub> are lower than today. Our results indicate that under such conditions, the surface ocean carbonate chemistry is expected to be more sensitive to a carbon perturbation (i.e. the PETM) due to lower CO<sub>3</sub><sup>2-</sup> concentration, whereas the deep ocean calcite sediments would be less vulnerable to dissolution due to the sluggish ocean.

## OBGC in the warm climate of the Late Paleocene

M. Heinze and T. Ilyina

Title Page

Abstract

Introduction

Conclusions

References

Tables

Figures



Back

Close

Full Screen / Esc

Printer-friendly Version

Interactive Discussion



## 1 Introduction

Recently, the Late Paleocene has received special interest because of its role as background climate for the Paleocene-Eocene Thermal Maximum (PETM), which could have been a possible analogue for present-day greenhouse warming and ocean acidification (e.g. Ridgwell and Zeebe, 2005; Zeebe and Zachos, 2013). The PETM describes a time period of about 170 kyr, which is characterized by an increase in mean surface temperatures of more than 5 °C (Kennett and Stott, 1991; Dickens et al., 1995; Zachos et al., 2008). During the PETM, the atmospheric CO<sub>2</sub> values increased significantly over a relatively short time period of about 10 kyr (Panchuk et al., 2008). Nonetheless, the question about the exact atmospheric CO<sub>2</sub> content before the PETM, as well as the maximum values of CO<sub>2</sub> during the PETM still remains unanswered (e.g. Pagani et al., 2006a).

The climate of the Late Paleocene was characterized by higher global average temperatures than in present-day, bearing ice-free conditions at the poles (Zachos et al., 2001). The pole-equator temperature gradient was smaller, displaying in sea surface temperatures (SST) of > 30 °C in the tropics (Pearson et al., 2001), and up to 20 °C in high latitudes (Sluijs et al., 2006; Lunt et al., 2012). Deep ocean waters were up to 10 °C warmer compared to modern values (Kennett and Stott, 1991; Zachos et al., 2001; Tripathi and Elderfield, 2005). The warmer climate and the Late Paleocene continental configuration influenced global ocean circulation patterns. The main deepwater formation occurred in southern high latitudes, with additional minor regions of deepwater formation in the Northern Hemisphere. There is no consensus if the Northern Hemisphere deepwater formation was stronger in the Atlantic or the Pacific (e.g. Bice and Marotzke, 2002; Tripathi and Elderfield, 2005; Nunes and Norris, 2006).

Hitherto, the focus of modeling the Late Paleocene with complex Earth System Models (ESM) was set to the physical ocean and atmospheric system (Huber and Sloan, 2001; Heinemann et al., 2009; Winguth et al., 2010). Studies about the PETM background climate show a wide range of inter-model variability, using prescribed

CPD

10, 1933–1975, 2014

### OBGC in the warm climate of the Late Paleocene

M. Heinze and T. Ilyina

Title Page

Abstract

Introduction

Conclusions

References

Tables

Figures



Back

Close

Full Screen / Esc

Printer-friendly Version

Interactive Discussion



**OBGC in the warm climate of the Late Paleocene**

M. Heinze and T. Ilyina

[Title Page](#)[Abstract](#)[Introduction](#)[Conclusions](#)[References](#)[Tables](#)[Figures](#)[Back](#)[Close](#)[Full Screen / Esc](#)[Printer-friendly Version](#)[Interactive Discussion](#)

atmospheric CO<sub>2</sub> concentrations ranging from 2× to 16× pre-industrial CO<sub>2</sub> (Lunt et al., 2012). Previous studies of the Late Paleocene ocean biogeochemistry are very rare and have been addressed exclusively with Earth System Models of intermediate complexity (EMIC) or box models (e.g. Panchuk et al., 2008; Zeebe et al., 2009; Ridgwell and Schmidt, 2010). These modeling studies are covering the whole PETM, with the major objective of constraining the absolute amount of the carbon perturbation. Their approach is based on reconstructions of the calcium carbonate compensation depth (CCD). By observing vertical shifts in the CaCO<sub>3</sub> dissolution horizons in sediment cores, before and after the peak of the event, rough estimates of the carbon perturbation during the PETM can be obtained. The depth of the pre-PETM CCD is still under discussion for wider geographical areas of the Late Paleocene oceans (Zeebe and Zachos, 2013). This leads to quite different estimates of total carbon mass and carbon injection speed into the climate system, necessary to obtain the observed sedimentary CaCO<sub>3</sub> dissolution (Dunkley Jones et al., 2010). Hence, the preceding conditions of ocean biogeochemistry are important for a realistic assessment of the PETM itself in order to gain knowledge about ocean biogeochemistry's influence on feedback mechanisms for the PETM, e.g. alterations in the carbonate buffer capacity. Yet, estimates of for instance, total alkalinity (TA) and dissolved inorganic carbon (DIC) during the Late Paleocene are not well known at present (Dunkley Jones et al., 2010).

In order to further constrain the state of the oceanic part of the carbon cycle during the Late Paleocene, we spin up and run the Hamburg Ocean Carbon Cycle model, HAMOCC, and the Max Planck Institute Ocean Model, MPIOM, under Late Paleocene boundary conditions into an equilibrium state. Based on Heinemann et al. (2009) we use a 560 ppm CO<sub>2</sub> Late Paleocene atmospheric forcing to achieve a plausible background climate for the PETM. The applied atmospheric CO<sub>2</sub> concentrations and Late Paleocene boundary conditions cause a new equilibrium climate state. Our study gives more detailed insights to the pre-PETM ocean biogeochemistry, since it is not only affected by modifications in temperature and atmospheric conditions at the ocean-atmosphere boundary (Archer et al., 2004), but also by alterations in the general

ocean physical state. We answer the question how the sluggish ocean state affects the oceanic part of the carbon cycle and how the general higher concentration of atmospheric CO<sub>2</sub> influences the carbonate chemistry.

The used model has been applied in a number of previous studies, simulating the pre-industrial, modern and future climate/ocean state, for example in the framework of the climate model intercomparison project (CMIP5; Ilyina et al., 2013). Therefore here we also use data of the CMIP5 experiments for comparison. This data is based on calculations with the Max Planck Institute for Meteorology-Earth System Model (MPI-ESM), for pre-industrial (1850–1879) climatic conditions.

In Sect. 2 of this paper we describe the model and give detailed information on the spin up of HAMOCC under Late Paleocene conditions. The general Late Paleocene climate state achieved by our simulation is presented in Sect. 3. Section 4 comprises the results of the modeled ocean biogeochemistry, followed by the conclusions in Sect. 5.

## 2 Model description and setup

### 2.1 The ocean biogeochemistry model HAMOCC

For our study we employ the Hamburg Ocean Carbon Cycle model (HAMOCC 5.1), which is based on Maier-Reimer (1993) and successive refinements (Maier-Reimer et al., 2005). HAMOCC simulates 18 biogeochemical tracers in the oceanic water column and 12 tracers in the upper 14 cm of the sediment. The tracers are simulated prognostically within a three-dimensional ocean circulation state. Tracer advection and mixing are computed by the Max Planck Institute ocean model (MPIOM) (Marsland et al., 2003; Jungclaus et al., 2013). Temperature, pressure and salinity of MPIOM are used to calculate various transformation rates and chemical constants within HAMOCC. The treatment of important biogeochemical processes in HAMOCC, related to this study, are being described in some more detail in the following paragraphs. For more complete information on HAMOCC, see Ilyina et al. (2013) and Maier-Reimer et al. (2005).

CPD

10, 1933–1975, 2014

## OBGC in the warm climate of the Late Paleocene

M. Heinze and T. Ilyina

Title Page

Abstract

Introduction

Conclusions

References

Tables

Figures



Back

Close

Full Screen / Esc

Printer-friendly Version

Interactive Discussion



## OBGC in the warm climate of the Late Paleocene

M. Heinze and T. Ilyina

Title Page

Abstract

Introduction

Conclusions

References

Tables

Figures

⏪

⏩

◀

▶

Back

Close

Full Screen / Esc

Printer-friendly Version

Interactive Discussion

Air–sea gas exchange is calculated for  $O_2$ ,  $CO_2$  and  $N_2$ . The air–sea  $CO_2$  flux is a result of the partial pressure difference between atmosphere and water, multiplied by a gas exchange rate and solubility according to Weiss (1974) and Groeger and Mikolajewicz (2011). It is then divided by the actual thickness of the surface layer. The velocity of the gas transfer depends on the Schmidt number and prognostic wind speed at the surface (Wanninkhof, 1992). The oceanic partial pressure of  $CO_2$  ( $pCO_2$ ) in the model is prognostically computed as a function of temperature, salinity, DIC, TA, and pressure.

Biological processes are described by an extended NPZD (Nutrient-Phytoplankton-Zooplankton-Detritus) type model (Six and Maier-Reimer, 1996). Primary production in HAMOCC is based on the co-limitation of phosphorous, nitrate and iron, as well as on temperature and radiation. The biogeochemistry related processes within the model are calculated on the basis of phosphorous. Associated changes between the remaining tracers are calculated using constant stoichiometric ratios (Redfield Ratio following Takahashi et al., 1985, P : N : C :  $-O_2$  ratio of 1 : 16 : 122 : 172). Phytoplankton is divided into silicifiers (opal shell) and calcifiers ( $CaCO_3$  shell). It is assumed that silicifiers are preferentially produced as long as silicate is available, which is shown by several observational studies (e.g. Lochte et al., 1993). Via prescribed vertical sinking rates opal,  $CaCO_3$  and particulate organic carbon (POC) are transported to depth. During the sinking, the particles undergo remineralization at a constant rate, distributing silicate, DIC, TA and nutrients (while decreasing oxygen) at depth. Remineralization of POC depends on oxygen. If oxygen falls below a concentration of  $0.5 \mu mol L^{-1}$  organic matter is decomposed by denitrification and sulphate reduction.

The formation of  $CaCO_3$  shells consumes DIC and TA in a molar ratio of 1 : 2. The dissolution of  $CaCO_3$  at depth is a function of the calcite saturation state ( $\Omega$ ) of sea water and a dissolution rate constant.  $\Omega$  is calculated from  $Ca^{2+}$  concentration in sea water, which is kept constant at  $10.3 mmol kg^{-1}$ ,  $CO_3^{2-}$  (carbonate ion) concentration and the apparent solubility product of calcite, based on temperature and pressure. Dissolution of opal takes place continuously over the whole water column with a rate of

0.01 d<sup>-1</sup>. Whereas CaCO<sub>3</sub> is less soluble in warm waters, the dissolution intensity of opal is positively correlated with temperature (Ragueneau et al., 2000).

The sediment module is based on Heinze and Maier-Reimer (1999) and Heinze et al. (1999). It basically calculates the same tracers as the water column model. The solid components of the sediment comprise opal, CaCO<sub>3</sub>, organic carbon and chemically inert dust (referred to from here onwards as “clay”). The tracer concentrations within the oceanic bottom layer and particularly the particle deposition from it determine the upper boundary for the sediment. The sediment reflects the uppermost 14 cm of the ocean floor and is resolved by 12 layers with increasing thickness and decreasing porosity from top to bottom. Below these layers, the model contains a diagenetically consolidated layer (burial). Major processes simulated in the sediment are vertical diffusion of porewater, decomposition of detritus, as well as dissolution of opal and CaCO<sub>3</sub>.

## 2.2 Topography and grid

The model setup is based on the interpolation of a Late Paleocene 2° × 2° topography, reconstructed by Bice and Marotzke (2001) (Fig. 1). It is used in several Paleocene-Eocene climate studies (Panchuk et al., 2008; Roberts et al., 2009; Heinemann et al., 2009; Zeebe, 2012). Main differences to present-day bathymetry lie in the open Central American Seaway, connecting the Atlantic and Pacific, as well as the existence of the Tethys Ocean and its connection to the Arctic Ocean, via Turgai strait. Although the Arctic Ocean has an additional link to the surrounding oceans, it lacks, unlike the present-day bathymetry, a deepwater connection. In the Southern Hemisphere, Drake Passage and Tasmanian Seaway are already open, but operate just as shallow water connections around Antarctica. The average ocean floor depth amounts to 3135 m (present-day setup: 3700 m) and has its deepest point at 5287 m (present-day setup: 5958 m) in the eastern equatorial Pacific. Vast areas of the Pacific are shallower in depths than in the modern ocean, the Atlantic is narrower than today and almost the whole Tethys does not exceed depths of 1000 m. It is mainly shaped by extended shelf

## OBGC in the warm climate of the Late Paleocene

M. Heinze and T. Ilyina

Title Page

Abstract

Introduction

Conclusions

References

Tables

Figures



Back

Close

Full Screen / Esc

Printer-friendly Version

Interactive Discussion



areas. Taken into account these differences, the model bathymetry yields a 14 % reduced sea water volume, compared to today's ocean.

In the conducted simulations HAMOCC integrates with a time step of 2.4 h (0.1 days). The horizontal resolution of the ocean model is  $3.5^\circ \times 3.5^\circ$  which equals a grid spacing from 70 km around South America to 430 km in the Pacific. The ocean model has 40 vertical layers, with increasing level thickness with depth: 9 layers are covering the upper 100 m and 23 layers the upper 1000 m of the water column. An orthogonal curvilinear grid is applied, with the poles located over northern Eurasia and South America to achieve best grid resolution for all ocean regions.

## 2.3 Forcing

In the ocean stand-alone model configurations atmospheric forcing has to be given. We use a Late Paleocene climate with an atmospheric  $\text{CO}_2$  concentration of 560 ppm, which is mimicked by an adequate atmospheric forcing, derived from Heinemann et al. (2009). The atmospheric conditions used in this study were calculated with a coupled climate model using ECHAM5, MPIOM and JSBACH in Paleocene-Eocene boundary conditions (560 ppm  $\text{CO}_2$ ). Atmospheric methane and nitrous oxide were set to pre-industrial values. The model showed after 2300 years of integration an equilibrium state in atmospheric and oceanic conditions (Heinemann et al., 2009). From the atmospheric model output we take 30 consecutive years from which we reproduce a daily mean Late Paleocene atmospheric forcing, based on the Ocean Model Intercomparison Project (OMIP) forcing used for present-day ocean-model-only setups (Roeske, 2006). The model is then forced using daily heat, freshwater and momentum fluxes in a 30 year cycle.

We initialize the stand-alone ocean model (MPIOM) based on the result of the 2300 years Late Paleocene equilibrium run by Heinemann et al. (2009). Additionally, we define a Paleocene climatology for ocean temperature and salinity from the same data. It displays the monthly mean climatological state for the two variables, averaged from daily data over a 30 year period. Sea surface salinity (SSS) and SST (upper 12 m)

CPD

10, 1933–1975, 2014

## OBGC in the warm climate of the Late Paleocene

M. Heinze and T. Ilyina

Title Page

Abstract

Introduction

Conclusions

References

Tables

Figures

◀

▶

◀

▶

Back

Close

Full Screen / Esc

Printer-friendly Version

Interactive Discussion



in our model are relaxed towards this Paleocene based climatology. Relaxation is taking place with a time constant of 180 days, it takes about 3 months till the surface layer is restored completely to the climatology.

## 2.4 Initialization of biogeochemistry

Using the MPIOM physical ocean state, we spin up HAMOCC starting from basin-wide-homogeneous distributions of biogeochemical tracers, taking pre-industrial concentrations as a rough orientation for spatial and vertical tracer distributions. We reduce the oceanic carbon inventory (from  $\sim 38\,500$  to  $\sim 32\,000$  Gt), as well as the different nutrient pools, proportional to the 14 % reduced ocean volume in the Late Paleocene setup. The reduction results in tracer concentrations close to modern values in the water column. Holding on to the reduced ocean volume bathymetry, allows a better comparison of the results to other models using this bathymetry (e.g. Panchuk et al., 2008; Heinemann et al., 2009).

The model is integrated for 3200 years, periodically repeating the forcing (see Sect. 2.3), while the inventories of TA are adjusted to the  $\text{CO}_2$  level of 560 ppm. Fluxes and tracer distribution stabilize after about 1000 model years within the water column. The distributions of tracers are not restored to any kind of data set, to be consistent with the biological, chemical, and physical dynamics of the model.

Since for the Late Paleocene the monthly mean dust deposition fields are not available (A. Winguth, personal communication, 2013), we prescribe a spatially homogeneous input of dust at the sea surface. The total amount of annual bio-available iron deposition to the ocean is the same as in the modern ocean setup ( $\sim 38 \times 10^{+7} \text{ kg Fe yr}^{-1}$ ; Mahowald et al., 2005). Besides the inventory adaptation and homogeneous dust deposition, the ocean chemistry in the Late Paleocene simulations is modeled the same as in modern MPI-ESM (Ilyina et al., 2013).

The weathering fluxes are adapted to the long-term sedimentation rates, used as a correction factor for balancing the different pools within the water column. The calcite weathering varies between 0 and  $900 \text{ kmol C s}^{-1}$ . Silicate weathering varies between 0

## OBGC in the warm climate of the Late Paleocene

M. Heinze and T. Ilyina

[Title Page](#)[Abstract](#)[Introduction](#)[Conclusions](#)[References](#)[Tables](#)[Figures](#)[Back](#)[Close](#)[Full Screen / Esc](#)[Printer-friendly Version](#)[Interactive Discussion](#)

to  $650 \text{ kmol Si s}^{-1}$ , and organic material varies from 0 to  $4 \text{ kmol C s}^{-1}$  during the spinup. After establishing an equilibrium state in the sediment, constant weathering fluxes are applied, as showed in Table 1.

## 2.5 Initialization of sediment

5 We initialize the sediment with 100% clay, while the  $\text{CaCO}_3$ , opal and organic carbon sediment pools start filling from first year on. While these long spin up simulations (50 kyr) have been done for present-day (e.g. Heinze et al., 1999), they do not exist for the Paleocene configuration. However, in matter of computing time it is not feasible to spin up the sediment module and achieve an equilibrium state within a realistic  
10 time frame. To circumvent this problem we use a computational method to accelerate processes within the sediment module of HAMOCC. This numerical tool works as following. The surface area of the sediment is reduced relating to its vertical axis/profile, by dividing the volume fraction of solid sediment and porewater by a prescribed acceleration factor. As the sediment cross section stays in its original extent, the same input  
15 rate affects now a reduced volume area. By maintenance of mass conservation the tracers are distributed faster throughout the sediment. The diffusion has to be reduced by the same factor to prevent overcompensation of the porewater. As soon as the sediment is saturated and is in equilibrium, the sediment module is extended to its original volume and area again. This sediment acceleration is turned on in year 1350, after  
20 having the water column tracers in an equilibrium state. The run proceeds using an acceleration factor of 1000. After approximately 150 years, the net-fluxes at the ocean-sediment boundary are strongly reduced and the sediment acceleration is turned off. In this way, accumulation of the sediment pool is equivalent to  $\sim 150\,000$  years of integration.

## OBGC in the warm climate of the Late Paleocene

M. Heinze and T. Ilyina

Title Page

Abstract

Introduction

Conclusions

References

Tables

Figures



Back

Close

Full Screen / Esc

Printer-friendly Version

Interactive Discussion



### 3 Late Paleocene climate state

The Late Paleocene climate state in our simulation is characterized by a global annual mean temperature of 23.56 °C (at 2 m height), using the atmospheric forcing described above (for comparison see Lunt et al., 2012). Maximum annual average temperatures are reached along the equator over Africa, Asia and South America with temperatures close to 40 °C (Fig. 2). The absolute annual average heat maximum lies over southern Asia (42.1 °C). Southern high latitudes (−1 °C at 90° S) are in annual average around 4 °C colder than northern high latitudes (3 °C at 90° N).

The prescribed wind forcing displays similar patterns as in the pre-industrial setup (not shown). However, the variability of Late Paleocene winds is much stronger than the variability of the pre-industrial state. Highest variability is found in the stormtrack regions in higher latitudes, while around the equator winds are comparable to pre-industrial. The atmospheric climate state has been evaluated in an earlier study using the same model version by Heinemann et al. (2009).

The ocean has a mean temperature of 14.68 °C (pre-industrial: 5.61 °C) and a global annual mean SST of 24.78 °C, which is in agreement with results of other climate models (Lunt et al., 2012). The northern high latitudes reach maximum SST's of 12.78 °C in Northern Hemisphere summer (JJA), but the sea surface of the central Arctic Ocean does not get warmer than 4 °C. The southern high latitudes show maximum SST of 17.83 °C in austral summer (DJF). In the presented setup there is no sea ice occurring, in each hemisphere winter the ocean stays completely ice free. The simulated high latitudes SST is in general agreement with the reconstructions for the Southern Ocean (Thomas et al., 2002), but do not fit the extreme proxy data assumptions of Sluijs et al. (2006) for the Arctic Ocean (for further discussion, see Heinemann et al., 2009). The meridional cross sections of the Pacific and the Atlantic Ocean (Fig. 3) differ from each other in their vertical temperature profiles. While the Atlantic features homogeneous relatively warm temperatures over largest parts of the water column, the temperature gradient in the Pacific is much more pronounced. Differences in deep sea temperatures

## OBGC in the warm climate of the Late Paleocene

M. Heinze and T. Ilyina

Title Page

Abstract

Introduction

Conclusions

References

Tables

Figures



Back

Close

Full Screen / Esc

Printer-friendly Version

Interactive Discussion





**OBGC in the warm climate of the Late Paleocene**

M. Heinze and T. Ilyina

Title Page

Abstract

Introduction

Conclusions

References

Tables

Figures



Back

Close

Full Screen / Esc

Printer-friendly Version

Interactive Discussion



Salinity and temperature profiles are mainly shaped by the meridional overturning circulation (MOC) (Fig. 4). The large-scale circulation structures are generally similar to modern conditions, but the Late Paleocene Atlantic is dominated by just one large scale circulation cell in our simulation (spreading nearly over the whole basin up to a depth of 4000 m), causing more homogeneous temperature and salinity distributions. The Atlantic Ocean lacks an AABW cell, while the AABW formation and spreading are much more pronounced in the Pacific. Here formation of deepwater occurs at 70° S. No further overturning takes place in the northern Pacific, as salinity concentrations in the surface ocean are too low, due to the Arctic Ocean water inflow. The Late Paleocene climate causes the ocean to be warmer on average (compared to pre-industrial conditions), leading to increased stratification throughout the water column. The reduced equator to pole temperature gradient results in a further slowdown of the MOC. Maximum deepwater formation (for depth > 900 m) of ~ 15 Sv occurs in the Southern Ocean and the North Atlantic (Fig. 4).

In MPIOM the mixed layer depth (MLD) is defined as the depth, where in situ density exceeds surface water density by more than  $0.125 \text{ kg m}^{-3}$  ( $\sigma_t$  criterion). The annual global mean MLD in the Late Paleocene setup levels at 52 m depth. Observations suggest an annual global mean of 65 m for MLD in present-day oceans (de Boyer Montegut et al., 2004). Since the MLD is interpreted as an indicator for the stratification of the ocean, which apparently is stronger in a warmer climate (e.g. Wetzels et al., 2006), the reduced MLD appears to be an expected result of our model simulation. As shown in Fig. 5 the MLD has a strong seasonal signal. In boreal winter deepwater formation is taking place in the North Atlantic. In austral winter the same deepening of MLD as an effect of convectational processes occurs in the South Pacific.

## 4 Late Paleocene ocean biogeochemistry

### 4.1 Air sea exchange processes

In this study we aimed at achieving steady-state conditions with respect to ocean biogeochemistry, in accordance with a long-term warm climate. Corresponding to the expectation of an equilibrium climate state, the annual mean CO<sub>2</sub> flux at the atmosphere–ocean boundary is balanced around zero. The global annual mean of surface ocean *p*CO<sub>2</sub> is 560 ppm within the Late Paleocene model setup. It shows highest values along the equator and in the eastern boundary currents, along South America in the Pacific, and Africa in the Atlantic (Fig. 6), similar to present-day (Takahashi et al., 2009). This reflects that its spacial distribution is mainly defined by temperature and salinity. The high *p*CO<sub>2</sub> areas result from upwelling of old water masses in these regions, induced by trade winds, bringing high CO<sub>2</sub> and nutrient rich waters to the surface.

The Atlantic Ocean is the major net-emitter of CO<sub>2</sub> with an annual outgassing of 0.41 Gt C, while the Pacific Ocean balances its net-fluxes around zero over the year. While high oceanic *p*CO<sub>2</sub> is associated with carbon release to the atmosphere, oceanic CO<sub>2</sub> uptake occurs in regions with low *p*CO<sub>2</sub> (if *p*CO<sub>2</sub>ocean < *p*CO<sub>2</sub>atm). The model computes lowest *p*CO<sub>2</sub> around Antarctica, especially close to Drake Passage, which corresponds to low salinity and TA concentrations in this area. Nevertheless, nearly the whole Southern Ocean (40–80° S) is characterized by *p*CO<sub>2</sub> values below the atmospheric CO<sub>2</sub> concentration of 560 ppm. This is consistent with deepwater formation and the deep MLD in austral winter in the Southern Ocean. Another prominent zone of low *p*CO<sub>2</sub> is located between 50° and 80° N, with its maximum in the North Atlantic and the North Pacific. Summarized over the whole year, the Arctic Ocean acts as a CO<sub>2</sub> sink (net-uptake of 0.06 Gt C). However, it plays a minor role in carbon uptake compared to present-day, due to the reduction in surface area of 40 % and increased ocean temperature. Instead, the Indian Ocean becomes the major driver in CO<sub>2</sub> net-uptake (0.31 Gt C yr<sup>-1</sup>). The southern part of the Indian Ocean is influenced by a deep mixed layer in austral winter (> 200 m), but even parts of the northern Indian Ocean show a MLD of up

**OBGC in the warm climate of the Late Paleocene**

M. Heinze and T. Ilyina

[Title Page](#)[Abstract](#)[Introduction](#)[Conclusions](#)[References](#)[Tables](#)[Figures](#)[Back](#)[Close](#)[Full Screen / Esc](#)[Printer-friendly Version](#)[Interactive Discussion](#)

to 80 m, resulting in rather low  $p\text{CO}_2$  values in the Indian Ocean surface waters. Consistent with the solubility effect, which declines with rising temperature (Weiss, 1974), our model shows that the equatorial regions in the Late Paleocene acted as a source for  $\text{CO}_2$ , while the high latitudes operate as a  $\text{CO}_2$  sink. This matches the present-day simulations with HAMOCC (Ilyina et al., 2013), but during the Late Paleocene it is mainly the Indian and Southern Ocean which compensates for the  $\text{CO}_2$  outgassing in the Atlantic.

Globally, the high ocean temperatures lead to a reduced solubility of  $\text{CO}_2$  in the surface ocean, compared to pre-industrial conditions. Moreover, the transfer of  $\text{CO}_2$  from the surface to intermediate and deep waters, by the oceanic velocity field is reduced by the sluggish circulation in the Late Paleocene. The sluggish circulation together with the weak ocean solubility pump, would act to reduce the ocean's uptake capacity of atmospheric  $\text{CO}_2$  in response to the carbon perturbation during the PETM.

## 4.2 Biological production and nutrients

Phosphate concentrations in the surface ocean show pronounced latitudinal gradients and weaker basin to basin differences in the Late Paleocene simulation. High phosphate concentrations characterize the surface ocean in the southern high latitudes, equatorial Pacific and Atlantic, as well as in Northern Hemisphere mid latitudes (Fig. 7). Strong equatorial upwelling of water masses in Atlantic and Pacific as well as moderate upwelling along the western coasts and in the Southern Ocean cause a maximum in phosphate surface concentrations in these regions. All other regions are characterized by phosphate-depletion, with the Atlantic and the Pacific gyres revealing the lowest phosphate concentrations in subtropical surface waters. Moreover, our simulation reveals a strong depletion in nutrients in the Arctic surface ocean, as a result of the interaction between bathymetry, stratification and freshwater input. The gradient in surface ocean phosphate concentration between low and high latitudes in the Southern Hemisphere resembles the modern one, despite the homogeneous dust/iron concentration prescribed for every grid cell. This indicates that the dust climatology is

not producing a strong signal in higher latitudes. Hence, in our Late Paleocene setup the iron limitation is not the major driving mechanism for preventing the surface ocean from complete consumption of nutrients, making the physical conditions at the poles accountable for it.

5 Surface oxygen concentration decreases from pole to equator, confirming its strong temperature dependency (Fig. 7). Generally higher SST than in modern conditions lead to slightly lower oxygen concentrations in the surface oceans. Only in the Arctic Ocean the low salinity is counteracting the temperature effect, as salinity is inversely related to oxygen solubility in seawater, according to Weiss (1970). This leads to similar oxygen  
10 concentrations/solubility like in the present-day setup.

While the physical dynamics and the biological production determine the surface concentrations of nutrients, the distribution of nutrients at depth is controlled by remineralization (Maier-Reimer, 1993). Modern nutrient and oxygen concentrations in the Pacific and Atlantic mirror the different age of the deepwater, defined by the global  
15 thermohaline circulation. In the Late Paleocene simulation the upper 1000 m of the water column reveal the maximum in phosphate concentrations in both basins, resulted by strong remineralization of organic matter, whereas the phosphate concentrations at depth are rather a product of global ocean circulation, then in situ remineralization. This explains the lower phosphate concentrations in the Atlantic over the Pacific, although OM export rates (in units per area) and oxygen concentrations are higher in the  
20 Atlantic. The oxygen concentration in Pacific deepwater is highly increased (Fig. 8), compared to modern conditions, which can be attributed to Southern Ocean deepwater formation and an enhanced exchange of Pacific and Atlantic through the Central American Seaway.

25 The oxygen minimum zones (OMZ) are very pronounced within the upper 1000 m in both basins. Oxygen concentrations are as low as  $20 \mu\text{mol kg}^{-1}$ , in meridional average, along the equatorial Atlantic and the North Pacific. The prominent OMZ's are attributed to the existence of productive equatorial zones (Fig. 9) (Norris et al., 2013) and reduced mixing in a more stagnant ocean during the Late Paleocene. For the Atlantic

**OBGC in the warm climate of the Late Paleocene**

M. Heinze and T. Ilyina

Title Page

Abstract

Introduction

Conclusions

References

Tables

Figures



Back

Close

Full Screen / Esc

Printer-friendly Version

Interactive Discussion



## OBGC in the warm climate of the Late Paleocene

M. Heinze and T. Ilyina

Title Page

Abstract

Introduction

Conclusions

References

Tables

Figures



Back

Close

Full Screen / Esc

Printer-friendly Version

Interactive Discussion

the low oxygen concentrations along the equator are even intensified in the meridional average, due to an additional high productivity zone along the northern continental margin of South America. In general the Atlantic shows an increase in OM export (in units per area) of nearly 60 % in comparison to pre-industrial. Although, the total export just increased by 13 %, due to the reduced area of the Atlantic in the Late Paleocene setup. However, the simulated OMZ's might be somewhat overestimated as illustrated in CMIP5 simulations. The model produces lower than observed oxygen concentrations, spreading over larger areas in the equatorial Pacific and along the western continental margin of Africa (Ilyina et al., 2013), which is typical for other global models as well (Andrews et al., 2013; Cocco et al., 2013).

The annual global primary production amounts to  $\sim 59$  GtC (Table 1) in the Late Paleocene simulation. The coastal upwelling regions along the western continental margins, as well as the equatorial regions of the Pacific and the Atlantic tend to be the dominant mechanism fueling primary production (Fig. 9). Compared to modern conditions, the production along the eastern boundary currents in Atlantic and Pacific is less pronounced. However, resulting from the open Central American Seaway, strong production arises along the northern tip of South America. The mid latitudes (nutrient poor mid latitudinal gyres) and the Arctic Ocean exhibit sparse productivity. On the contrary the nutrient rich Southern Ocean is responsible for  $\sim 11$  % of the global primary production.

The production of calcite shells follows the low silicate surface concentrations in the Atlantic, Tethys and Indian Ocean, as well as in the western equatorial Pacific. Regions of higher silicate concentrations which correspond to upwelling locations, are dominated by production of opal shells as implied from our modeling approach.

The export production of  $\text{CaCO}_3$  is with  $0.63 \text{ GtCyr}^{-1}$  lower than for pre-industrial conditions (see Table 1). This leads to a  $\text{CaCO}_3$  : POC export ratio of 0.07, contrary to the PETM simulations of Panchuk et al. (2008) and Ridgwell and Schmidt (2010) suggesting a ratio of 0.2. As the  $\text{CaCO}_3$  : POC rain ratio is an important source of uncertainty, controlling the sedimentary  $\text{CaCO}_3$  wt% distribution, Panchuk et al. (2008)

**OBGC in the warm  
climate of the Late  
Paleocene**

M. Heinze and T. Ilyina

Title Page

Abstract

Introduction

Conclusions

References

Tables

Figures

⏪

⏩

◀

▶

Back

Close

Full Screen / Esc

Printer-friendly Version

Interactive Discussion



base their suggestion on an ensemble run using different export ratios. Finally, 0.2 matches best their pre-PETM CCD (3.5–4 km depth) and  $\text{CaCO}_3$  sediment distribution. Simulations for present-day export ratio suggest that the ratio levels more around 0.1 ( $\sim 0.06$  Sarmiento et al., 2002;  $\sim 0.1$  CMIP5 runs MPI-ESM;  $< 1.4$  Ridgwell and Schmidt, 2010). In our simulation the  $\text{CaCO}_3$  : POC export ratio is a result of production, remineralization and sinking velocity. Because dissolution of opal is positively correlated with temperature, in a warmer ocean more silica is available for opal production in the upper ocean (Fig. 8). This indirectly results in less  $\text{CaCO}_3$  formation in our model set up. The homogeneous dust (iron) climatology can not cause a shift from  $\text{CaCO}_3$  towards opal producing skeletons. Thus it can only lead to an absolute increase in production of former iron-limiting low productivity zones, but not change the proportions between the two building materials.

An interbasinal comparison reveals increased overall export fluxes in the Atlantic. Opal,  $\text{CaCO}_3$  and POC export (in units per area) even exceed the ones in the Pacific. However, in absolute numbers the Pacific Ocean is the main driver, covering about 50 % of the global ocean surface area it is responsible for  $> 50$  % of POC export ( $4.55 \text{ GtCyr}^{-1}$ ), globally. The strong depletion in silica in Tethys surface waters (Fig. 8) favours high  $\text{CaCO}_3$  production. As a consequence parts of the Tethys ocean shows low surface TA. The Tethys has just a minor impact on the strength of the biological carbon pump, exporting  $0.28 \text{ GtCyr}^{-1}$ .

### 4.3 Carbonate chemistry

TA concentrations decrease from the equator towards the poles, with the subtropical gyres showing both, elevated DIC and TA, compared to the surrounding surface waters (Fig. 10). The spatial patterns of surface ocean DIC and TA reproduced by the model are similar to pre-industrial conditions. Highest DIC concentrations, besides the gyres, are located in the Southern Ocean ( $2100 \mu\text{mol kg}^{-1}$ ) whereas the Arctic Ocean exhibits low DIC concentrations around  $1800 \mu\text{mol kg}^{-1}$ . While the SST determines mainly the surface distribution of DIC, the surface TA is rather reflecting the structure of salinity

## OBGC in the warm climate of the Late Paleocene

M. Heinze and T. Ilyina

Title Page

Abstract

Introduction

Conclusions

References

Tables

Figures

⏪

⏩

◀

▶

Back

Close

Full Screen / Esc

Printer-friendly Version

Interactive Discussion



(Maier-Reimer, 1993), which is shaped by the precipitation-evaporation gradients, leading to increased TA concentrations in the subtropics. Low salinity in the Arctic Ocean, induced by the poor internal mixing and the low exchange with the surrounding oceans (no deep-water exchange) is driving the TA to very low values ( $< 1800 \mu\text{mol kg}^{-1}$ ). High SST, low TA, and little  $\text{CO}_2$  uptake in the Arctic Ocean result in generally low DIC concentrations over the whole water column, reducing the Arctic Ocean's carbon storage capacity.

The surface seawater  $\text{CO}_3^{2-}$  concentration is shaped by the elevated atmospheric  $\text{CO}_2$  concentration of 560 ppm. Higher atmospheric  $\text{CO}_2$  concentrations do not have an impact on TA, but cause a shift from  $\text{CO}_3^{2-}$  to  $\text{HCO}_3^-$  (bicarbonate). The reduced  $\text{CO}_3^{2-} : \text{DIC}$  ratio which is characterizing the pre-PETM carbonate chemistry is reducing the oceanic buffer capacity towards atmospheric  $\text{CO}_2$  perturbations.

In the vertical profile the maximum in DIC concentration around the equator, spreading from 400 to 1000 m depth (Fig. 10), is related to biological processes. It marks the depth in which intense dissolution/remineralization of the exported particles takes place. The remineralization of POC is releasing DIC and consuming oxygen, while at the same time the dissolution of  $\text{CaCO}_3$  is increasing the TA at  $\sim 1000$  m depth (Fig. 10). That the Atlantic exhibits higher TA and DIC concentrations over the Pacific can be explained by the stronger export of  $\text{CaCO}_3$  and POC (in units per area). In the uppermost layers of the ocean, the difference in  $\text{CO}_3^{2-}$  concentration between Atlantic and Pacific is not evident anymore. The atmospheric  $\text{CO}_2$  concentration of 560 ppm causes low  $\text{CO}_3^{2-}$  concentrations, reaching up to a depth of 600 m in both oceans. In layers beneath 2000 m the  $\text{CO}_3^{2-}$  concentrations within the basins show homogeneous distributions, with the Atlantic  $\text{CO}_3^{2-}$  concentrations ( $100\text{--}120 \mu\text{mol kg}^{-1}$ ) being nearly twice as high as in the Pacific ( $60\text{--}70 \mu\text{mol kg}^{-1}$ ).

The calculated global average pH in the surface ocean amounts to 7.9, which is in agreement with the estimate by Tyrrell and Zeebe (2004) and close to the suggestion of Ridgwell and Schmidt (2010), that Late Paleocene pH surface values were  $\sim 0.4$  lower

than today. The surface distribution in pH displays a similar pattern as we know from pre-industrial pH, albeit at lower values. Within the upwelling areas along the equator and in front of the western continental margins the pH is lower than in the mid latitudes. The Arctic Ocean shows particularly low pH, correlated to the very low salinities.

At depth large parts of the Pacific are undersaturated with respect to  $\text{CaCO}_3$  (Fig. 11). However, the undersaturation is characterized by a strong gradient in the east-west direction, which is not evident in the zonally averaged  $\Omega$  values (Fig. 11). The basin wide undersaturation in the Pacific starts below a depth of 3700 m. The horizontal gradient in  $\Omega$  is even enhanced by inflow of  $\text{CO}_3^{2-}$  rich water from the Indian Ocean and undersaturated ( $\Omega < 1$ ) near-surface waters in the eastern part of the basin. Undersaturation occurs due to biological respiration processes in intermediate waters, which correlate to very low pH values of up to 6.9, computed for the uppermost 1000 m of the water column within the equatorial Pacific.

The elevated ocean temperatures during the late Paleocene produce a lower  $\text{CO}_3^{2-}$  saturation concentration, because it inversely depends on temperature. This should lead to an increased  $\Omega$ , in comparison to present-day, as formerly discussed in Zeebe and Zachos (2007). This effect is strong in the Atlantic, which is at depth in average around 5 °C warmer than the Pacific in our simulation. Here, a reduced calcite saturation concentration counteracts the lower  $\text{CO}_3^{2-}$  concentrations. The undersaturation with respect to  $\text{CO}_3^{2-}$  in the equatorial Atlantic between 200–1000 m depth is a result of very low pH in the low latitudes subsurface ocean, caused by aerobe and anaerobe remineralization (Fig. 8). The North Atlantic and the Indian Ocean show no undersaturation with respect to  $\text{CaCO}_3^{2-}$  at all.

Our approach provides  $\Omega$  distributions being consistent with the 3-d hydrodynamical field and the biogeochemical processes as simulated for the Late Paleocene ocean. We perceive a complex pattern of  $\Omega$ , which includes e.g. undersaturated waters in shallower depth overlying supersaturated waters in deeper layers, as seen in the Pacific in our simulation. Local undersaturation might be of importance since 60 to 80 % of the  $\text{CaCO}_3$  export is dissolved already in the upper 1000 m of the water column, as shown

**OBGC in the warm climate of the Late Paleocene**

M. Heinze and T. Ilyina

Title Page

Abstract

Introduction

Conclusions

References

Tables

Figures



Back

Close

Full Screen / Esc

Printer-friendly Version

Interactive Discussion



**OBGC in the warm climate of the Late Paleocene**

M. Heinze and T. Ilyina

[Title Page](#)[Abstract](#)[Introduction](#)[Conclusions](#)[References](#)[Tables](#)[Figures](#)[⏪](#)[⏩](#)[◀](#)[▶](#)[Back](#)[Close](#)[Full Screen / Esc](#)[Printer-friendly Version](#)[Interactive Discussion](#)

by present-day studies (Feely et al., 2004; Ilyina and Zeebe, 2012). The assumption of a uniform basinwide saturation horizon (depth where  $\Omega = 1$ ) or lysocline (depths where  $\Omega = 0.8$ ; Ridgwell and Zeebe, 2005) for the Late Paleocene oceans (e.g. Panchuk et al., 2008; Zeebe et al., 2009; Cui et al., 2011) as it has been made for several EMIC and box model studies might underestimate these dissolution processes.

#### 4.4 Sediment composition

The sediment compartment was initialized with 100 % clay. Hence, the resulting distribution of organic matter, opal and  $\text{CaCO}_3$  in the sediment reflects water column processes. Large sedimentary opal deposits are located in the equatorial Pacific, along the eastern boundary currents and in the Southern Ocean. This mirrors the nutrient rich upwelling areas, zones where high production at the surface takes place. However, it is noticeable that the annual net sedimentation rate of opal is very small on the global scale. Since the opal remineralization rate is positively correlated with temperature, we attribute this effect to the increased deep sea temperature as compared to the pre-industrial setup of the model.

$\text{CaCO}_3$  deposits cover wider areas, corresponding to supersaturated ( $\Omega > 1$ ) bottom waters and  $\text{CaCO}_3$  production at the surface. Present-day apparent predominance of  $\text{CaCO}_3$  accumulation in the Atlantic and Indian Ocean compared to the Pacific is also preserved in the Late Paleocene simulations. A greater degree of undersaturation in the deep Pacific exists as a consequence of metabolic  $\text{CO}_2$  accumulation (Ridgwell and Zeebe, 2005). Unlike today, the Arctic and Southern Ocean bear  $\text{CaCO}_3$  deposits, attributed to a regionally higher  $\text{CaCO}_3$  : POC rain ratio and less corrosive bottom waters in these regions.

The upper 14 cm of the sediment being affected by dissolution processes contain a total  $\text{CaCO}_3$  amount of 2049 GtC. This corresponds to a global average  $\text{CaCO}_3$  wt% of 36. The absolute amount of sedimentary  $\text{CaCO}_3$  in our simulation is slightly higher than estimates for present-day (1610 GtC, CMIP5 simulation with MPI-ESM; 1770 GtC, Archer et al., 1998). Another model study results in a lower total  $\text{CaCO}_3$

amount of 800 Gt C for present-day and a decrease to 620 Gt C for a pre-PETM setup (Zeebe, 2012).

Panchuk et al. (2008) evaluate their computed  $\text{CaCO}_3$  distribution by a compilation of late Paleocene marine sediment cores. Our model result captures the spatial pattern and the absolute values of the compiled sediment core data relatively well, yet our model calculates a much smaller  $\text{CaCO}_3$ :POC rain ratio. Differences between Panchuk et al. (2008) and our estimates persist in the absence of  $\text{CaCO}_3$  in the central Pacific, as well as in the abundance of  $\text{CaCO}_3$  in the North Atlantic in our results. This could be due to the different locations for Northern Hemisphere deepwater formation, which is located in the North Pacific in Panchuk et al. (2008), but in the North Atlantic in our simulation. Based on the data of Panchuk et al. (2008) one can not discriminate the validity of the two model results. Due to the lack of sediment cores in the North Atlantic, both  $\text{CaCO}_3$  distributions/abundances seem to be plausible.

## 5 Summary and conclusions

Using the biogeochemistry model HAMOCC coupled with the ocean general circulation model MPIOM we establish a steady-state ocean biogeochemistry simulation with Late Paleocene boundary conditions. We present spatial and vertical tracer distributions within a warmer climate and display how the Late Paleocene ocean physical state influences the biogeochemistry. We provide a general overview of major oceanic carbon cycle components in a high  $\text{CO}_2$  (560 ppm) world and give estimates of the PETM background climate.

The Late Paleocene simulation reveals a strong stratification of water masses, which is displayed by temperature and salinity profiles, as well as the shallow MLD. These conditions are also found in other coupled atmosphere–ocean general circulation models using Eocene boundary conditions (Lunt et al., 2010). The sluggish circulation affects the atmosphere–ocean exchange fluxes of  $\text{CO}_2$  by shifting its spatial patterns, i.e. uptake in the Indian and Southern Ocean compensates the  $\text{CO}_2$  outgassing of the

CPD

10, 1933–1975, 2014

## OBGC in the warm climate of the Late Paleocene

M. Heinze and T. Ilyina

Title Page

Abstract

Introduction

Conclusions

References

Tables

Figures

⏪

⏩

◀

▶

Back

Close

Full Screen / Esc

Printer-friendly Version

Interactive Discussion



**OBGC in the warm climate of the Late Paleocene**

M. Heinze and T. Ilyina

[Title Page](#)[Abstract](#)[Introduction](#)[Conclusions](#)[References](#)[Tables](#)[Figures](#)[Back](#)[Close](#)[Full Screen / Esc](#)[Printer-friendly Version](#)[Interactive Discussion](#)

Atlantic Ocean. Furthermore also the strength of the different oceanic carbon pumps is affected by a more stagnant circulation. In comparison to present-day conditions, the solubility pump is weaker due to the elevated SST and the vertical transfer of carbon from surface to intermediate and deep waters is slowed down. Nevertheless, the enhanced ocean stratification is not prominent enough to prevent the supply of nutrients to surface waters and hence the global primary production is only slightly decreased.

The intensification of primary production along the equator causes enhanced remineralization within the upper 1000 m of the Atlantic and Pacific, leading to strong OMZ's. The global pattern in oxygen distribution in the intermediate and deep waters is affected by the altered continental configuration. In particular the open Central American Seaway and deepwater formation in the South Pacific ensure the adjustment between Atlantic and Pacific oxygen concentrations.

Our results indicate that an equilibrium  $\text{CO}_2$  exchange during Late Paleocene can be established without increased concentrations of TA, as assumed by Pearson and Palmer (2000), while the calculated surface ocean pH (lower than today) is in agreement with the results of Tyrrell and Zeebe (2004) and Ridgwell and Schmidt (2010). Low surface TA concentrations are positively influenced by a lower  $\text{CaCO}_3$ : opal export ratio, since less carbonate leaves the surface ocean. This effect is associated with the temperature dependent remineralization of opal, which produces an increased silicate/opal turnover rate. The simulated export ratio lies within the range of estimates for modern conditions (Schneider et al., 2008), but falls below the estimates given by the simulations of Panchuk et al. (2008) and Ridgwell and Schmidt (2010), covering the Paleocene-Eocene period. This difference may be a result of using quite different type of models.

While the Pacific deepwater is widely undersaturated with respect to  $\text{CaCO}_3$ , the Atlantic does not show any  $\text{CaCO}_3$  undersaturation in depth beneath 1000 m. We claim that the warm temperatures in the deep Atlantic are responsible for producing a too weak saturation gradient (by decreasing saturation concentration) compared to other

studies (e.g. Zeebe et al., 2009). The surface ocean is characterized by globally lower  $\text{CO}_3^{2-}$  concentrations than today, because of higher atmospheric  $\text{CO}_2$  concentrations.

In terms of sensitivity of the carbonate chemistry to a large carbon perturbation, as it is estimated for the PETM, Late Paleocene climatic conditions seem to have opposing effects. The lower surface ocean  $\text{CO}_3^{2-} : \text{DIC}$  ratio reduces carbonate buffer capacity and results in higher sensitivity towards additional  $\text{CO}_2$ . Yet, the reduced  $\text{CaCO}_3 : \text{opal}$  export ratio counteracts this effect at least partially, in our simulation. In greater depth, the decreased  $\text{CaCO}_3$  saturation concentration (i.e. increased  $\Omega$ ) would reduce the sedimentary  $\text{CaCO}_3$  dissolution. Furthermore, the warm and stratified ocean would reduce the amount of  $\text{CO}_2$  reacting with seawater and being transported into the deep ocean already beforehand.

*Acknowledgements.* We thank H. Haak who helped with the setup of the model and M. Heinemann who provided data for producing a Late Paleocene atmospheric forcing. We wish to thank K. Six for advice and helpful comments on the manuscript. The authors acknowledge the late E. Maier-Reimer for valuable insights on the model.

The service charges for this open access publication have been covered by the Max Planck Society.

## References

- Andrews, O. D., Bindoff, N. L., Halloran, P. R., Ilyina, T., and Le Quéré, C.: Detecting an external influence on recent changes in oceanic oxygen using an optimal fingerprinting method, *Biogeosciences*, 10, 1799–1813, doi:10.5194/bg-10-1799-2013, 2013. 1949
- Archer, D., Kheshgi, H., and Maier-Reimer, E.: Dynamics of fossil fuel  $\text{CO}_2$  neutralization by marine  $\text{CaCO}_3$ , *Global Biogeochem. Cy.*, 12, 259–276, doi:10.1029/98GB00744, 1998. 1953
- Archer, D., Martin, P., Buffett, B., Brovkin, V., Rahmstorf, S., and Ganopolski, A.: The importance of ocean temperature to global biogeochemistry, *Earth Planet. Sc. Lett.*, 222, 333–348, 2004. 1936

## OBGC in the warm climate of the Late Paleocene

M. Heinze and T. Ilyina

Title Page

Abstract

Introduction

Conclusions

References

Tables

Figures



Back

Close

Full Screen / Esc

Printer-friendly Version

Interactive Discussion



**OBGC in the warm climate of the Late Paleocene**

M. Heinze and T. Ilyina

[Title Page](#)[Abstract](#)[Introduction](#)[Conclusions](#)[References](#)[Tables](#)[Figures](#)[◀](#)[▶](#)[◀](#)[▶](#)[Back](#)[Close](#)[Full Screen / Esc](#)[Printer-friendly Version](#)[Interactive Discussion](#)

- Bice, K. L. and Marotzke, J.: Numerical evidence against reversed thermohaline circulation in the warm Paleocene/Eocene ocean, *J. Geophys. Res.*, 106, 11529–11542, doi:10.1029/2000JC000561, 2001. 1939
- Bice, K. L. and Marotzke, J.: Could changing ocean circulation have destabilized methane hydrate at the Paleocene/Eocene boundary?, *Paleoceanography*, 17, 1018–1033, doi:10.1029/2001PA000678, 2002. 1935
- Cocco, V., Joos, F., Steinacher, M., Frölicher, T. L., Bopp, L., Dunne, J., Gehlen, M., Heinze, C., Orr, J., Oeschies, A., Schneider, B., Segschneider, J., and Tjiputra, J.: Oxygen and indicators of stress for marine life in multi-model global warming projections, *Biogeosciences*, 10, 1849–1868, doi:10.5194/bg-10-1849-2013, 2013. 1949
- Cui, Y., Kump, L. R., Ridgwell, A. J., Charles, A. J., Junium, C. K., Diefendorf, A. F., Freeman, K. H., Urban, N. M., and Harding, I. C.: Slow release of fossil carbon during the Palaeocene-Eocene Thermal Maximum, *Nat. Geosci.*, 4, 481–485, doi:10.1038/ngeo1179, 2011. 1953
- de Boyer Montegut, C., Madec, G., Fischer, A. S., Lazar, A., and Iudicone, D.: Mixed layer depth over the global ocean: An examination of profile data and a profile-based climatology, *J. Geophys. Res.*, 109, C12003, doi:10.1029/2004JC002378, 2004. 1945
- Dickens, G. R., O’Neil, J. R., Rea, D. K., and Owen, R. M.: Dissociation of oceanic methane hydrate as a cause of the carbon isotope excursion at the end of the, *Paleocene Paleoceno.*, 10, 965–971, 1995. 1935
- Dunkley Jones, T., Ridgwell, A., Lunt, D. J., Maslin, M. A., Schmidt, D. N., and Valdes, P. J.: A Palaeogene perspective on climate sensitivity and methane hydrate instability, *Philos. T. Roy. Soc. A*, 368, 2395–2415, doi:10.1098/rsta.2010.0053, 2010. 1936
- Feely, R. A., Sabine, C. L., Lee, K., Berelson, W., Kleypas, J., Fabry, V. J., and Millero, F. J.: Impact of anthropogenic CO<sub>2</sub> on the CaCO<sub>3</sub> system in the oceans, *Science*, 305, 362–366, 2004. 1953
- Groeger, M. and Mikolajewicz, U.: Note on the CO<sub>2</sub> air–sea gas exchange at high temperatures, *Ocean Model.*, 39, 284–290, 2011. 1938
- Heinemann, M., Jungclaus, J. H., and Marotzke, J.: Warm Paleocene/Eocene climate as simulated in ECHAM5/MPI-OM, *Clim. Past*, 5, 785–802, doi:10.5194/cp-5-785-2009, 2009. 1935, 1936, 1939, 1940, 1941, 1943

## OBGC in the warm climate of the Late Paleocene

M. Heinze and T. Ilyina

Title Page

Abstract

Introduction

Conclusions

References

Tables

Figures

◀

▶

◀

▶

Back

Close

Full Screen / Esc

Printer-friendly Version

Interactive Discussion

Heinze, C. and Maier-Reimer, E.: The Hamburg Oceanic Carbon Cycle Circulation Model version “HAMOCC2s” for Longtime Integrations, Technical Report 20, Deutsches Klimarechenzentrum, Modellberatungsgruppe, Hamburg, 1999. 1939

Heinze, C., Maier-Reimer, E., Winguth, A. M. E., and Archer, D.: A global oceanic sediment model for long-term climate studies, *Global Biogeochem. Cy.*, 13, 221–250, doi:10.1029/98GB02812, 1999. 1939, 1942

Huber, M. and Sloan, L. C.: Heat transport, deep waters, and thermal gradients: coupled simulation of an Eocene greenhouse climate, *Geophys. Res. Lett.*, 28, 3481–3484, 2001. 1935

Ilyina, T. and Zeebe, R. E.: Detection and projection of carbonate dissolution in the water column and deep-sea sediments due to ocean acidification, *Geophys. Res. Lett.*, 39, L06606, doi:10.1029/2012GL051272, 2012. 1953

Ilyina, T., Six, K. D., Segsneider, J., Maier-Reimer, E., Li, H., and Núñez-Riboni, I.: Global ocean biogeochemistry model HAMOCC: Model architecture and performance as component of the MPI-Earth system model in different CMIP5 experimental realizations, *J. Adv. Model. Earth Syst.*, 5, 287–315, doi:10.1029/2012MS000178, 2013. 1937, 1941, 1947, 1949

Jungclaus, J. H., Fischer, N., Haak, H., Lohmann, K., Marotzke, J., Matei, D., Mikolajewicz, U., Notz, D., and von Storch, J. S.: Characteristics of the ocean simulations in the Max Planck Institute Ocean Model (MPIOM) the ocean component of the MPI-Earth system model, *J. Adv. Model. Earth Syst.*, 5, 422–446, doi:10.1002/jame.20023, 2013. 1937

Kennett, J. P. and Stott, L. D.: Abrupt deep-sea warming, palaeoceanographic changes and benthic extinctions at the end of the Palaeocene, *Nature*, 353, 225–229, doi:10.1038/353225a0, 1991. 1935

Lochte, K., Ducklow, H., Fasham, M., and Stienen, C.: Plankton succession and carbon cycling at 47° N 20° W during the JGOFS North Atlantic Bloom Experiment, *Deep-Sea Res. Pt. II*, 40, 91–114, 1993. 1938

Lunt, D. J., Valdes, P. J., Jones, T. D., Ridgwell, A., Haywood, A. M., Schmidt, D. N., Marsh, R., and Maslin, M.: CO<sub>2</sub>-driven ocean circulation changes as an amplifier of Paleocene-Eocene thermal maximum hydrate destabilization, *Geology*, 38, 875–878, 2010. 1954

Lunt, D. J., Dunkley Jones, T., Heinemann, M., Huber, M., LeGrande, A., Winguth, A., Loptson, C., Marotzke, J., Roberts, C. D., Tindall, J., Valdes, P., and Winguth, C.: A model–data comparison for a multi-model ensemble of early Eocene atmosphere–ocean simulations: EoMIP, *Clim. Past*, 8, 1717–1736, doi:10.5194/cp-8-1717-2012, 2012. 1935, 1936, 1943

## OBGC in the warm climate of the Late Paleocene

M. Heinze and T. Ilyina

Title Page

Abstract

Introduction

Conclusions

References

Tables

Figures

◀

▶

◀

▶

Back

Close

Full Screen / Esc

Printer-friendly Version

Interactive Discussion

- Mahowald, N. M., Baker, A. R., Bergametti, G., Brooks, N., Duce, R. A., Jickells, T. D., Kubilay, N., Prospero, J. M., and Tegen, I.: Atmospheric global dust cycle and iron inputs to the ocean, *Global Biogeochem. Cy.*, 19, GB4025, doi:10.1029/2004GB002402, 2005. 1941
- Maier-Reimer, E.: Geochemical cycles in an ocean general circulation model, preindustrial tracer distributions, *Global Biogeochem. Cy.*, 7, 645–677, doi:10.1029/93GB01355, 1993. 1937, 1948, 1951
- Maier-Reimer, E., Kriest, I., Segschneider, J., and Wetzol, P.: The HAMBURG Ocean Carbon Cycle Model HAMOCC 5.1, Technical Description Release 1.1, Tech. rep. 14, Reports on Earth System Science, Hamburg, Germany, 2005. 1937
- Marsland, S., Haak, H., Jungclaus, J., Latif, M., and Röske, F.: The Max-Planck-Institute global ocean/sea ice model with orthogonal curvilinear coordinates, *Ocean Model.*, 5, 91–127, 2003. 1937
- Norris, R. D., Turner, S. K., Hull, P. M., and Ridgwell, A.: Marine ecosystem responses to cenozoic global change, *Science*, 341, 492–498, doi:10.1126/science.1240543, 2013. 1948
- Nunes, F. and Norris, R. D.: Abrupt reversal in ocean overturning during the Palaeocene/Eocene warm period, *Nature*, 439, 60–63, 2006. 1935
- Pagani, M., Caldeira, K., Archer, D., and Zachos, J. C.: An ancient carbon mystery, *Science*, 314, 1556–1557, doi:10.1126/science.1136110, 2006a. 1935
- Pagani, M., Pedentchouk, N., Huber, M., Sluijs, A., Schouten, S., Brinkhuis, H., Sinninghe Damste, J. S., Dickens, G. R., Backman, J., Clemens, S., Cronin, T., Eynaud, F., Gattacceca, J., Jakobsson, M., Jordan, R., Kaminski, M., King, J., Koc, N., Martinez, N. C., Matthiessen, J., McInroy, D., Moore, T. C., Moran, K., O'Regan, M., Onodera, J., Palike, H., Rea, B., Rio, D., Sakamoto, T., Smith, D. C., Stein, R., St John, K. E. K., Suto, I., Suzuki, N., Takahashi, K., Watanabe, M., and Yamamoto, M.: Arctic hydrology during global warming at the Palaeocene/Eocene thermal maximum, *Nature*, 443, 598–598, doi:10.1038/nature05211, 2006b. 1944
- Panchuk, K., Ridgwell, A., and Kump, L.: Sedimentary response to Paleocene-Eocene Thermal Maximum carbon release: a model-data comparison, *Geology*, 36, 315–318, doi:10.1130/G24474A.1, 2008. 1935, 1936, 1939, 1941, 1949, 1953, 1954, 1955
- Pearson, P. N. and Palmer, M. R.: Atmospheric carbon dioxide concentrations over the past 60 million years, *Nature*, 406, 695–699, doi:10.1038/35021000, 2000. 1955

**OBGC in the warm  
climate of the Late  
Paleocene**

M. Heinze and T. Ilyina

[Title Page](#)[Abstract](#)[Introduction](#)[Conclusions](#)[References](#)[Tables](#)[Figures](#)[⏪](#)[⏩](#)[◀](#)[▶](#)[Back](#)[Close](#)[Full Screen / Esc](#)[Printer-friendly Version](#)[Interactive Discussion](#)

- Pearson, P. N., Ditchfield, P. W., Singano, J., Harcourt-Brown, K. G., Nicholas, C. J., Olson, R. K., Shackleton, N. J., and Hall, M. A.: Warm tropical sea surface temperatures in the Late Cretaceous and Eocene epochs, *Nature*, 413, 481–487, doi:10.1038/35097000, 2001. 1935
- 5 Ragueneau, O., Tréguer, P., Leynaert, A., Anderson, R., Brzezinski, M., DeMaster, D., Dugdale, R., Dymond, J., Fischer, G., Francois, R., Heinze, C., Maier-Reimer, E., Martin-Jezequel, V., Nelson, D., and Queguiner, B.: A review of the Si cycle in the modern ocean: recent progress and missing gaps in the application of biogenic opal as a paleoproductivity proxy, *Global Planet. Change*, 26, 317–365, 2000. 1939
- 10 Ridgwell, A. and Schmidt, D.: Past constraints on the vulnerability of marine calcifiers to massive carbon dioxide release, *Nat. Geosci.*, 3, 196–200, 2010. 1936, 1949, 1950, 1951, 1955
- Ridgwell, A. and Zeebe, R.: The role of the global carbonate cycle in the regulation and evolution of the Earth system, *Earth Planet. Sc. Lett.*, 234, 299–315, 2005. 1935, 1953
- 15 Roberts, C. D., LeGrande, A. N., and Tripati, A. K.: Climate sensitivity to Arctic seaway restriction during the early Paleogene, *Earth Planet. Sc. Lett.*, 286, 576–585, 2009. 1939
- Roeske, F.: A global heat and freshwater forcing dataset for ocean models, *Ocean Model.*, 11, 235–297, 2006. 1940
- Sarmiento, J. L., Dunne, J., Gnanadesikan, A., Key, R. M., Matsumoto, K., and Slater, R.: A new estimate of the CaCO<sub>3</sub> to organic carbon export ratio, *Global Biogeochem. Cy.*, 16, 54-1–54-12, doi:10.1029/2002GB001919, 2002. 1950
- 20 Schneider, B., Bopp, L., Gehlen, M., Segschneider, J., Frölicher, T. L., Cadule, P., Friedlingstein, P., Doney, S. C., Behrenfeld, M. J., and Joos, F.: Climate-induced interannual variability of marine primary and export production in three global coupled climate carbon cycle models, *Biogeosciences*, 5, 597–614, doi:10.5194/bg-5-597-2008, 2008. 1955
- 25 Six, K. and Maier-Reimer, E.: Effects of plankton dynamics on seasonal carbon fluxes in an ocean general circulation model, *Global Biogeochem. Cy.*, 10, 559–583, 1996. 1938
- Sluijs, A., Schouten, S., Pagani, M., Woltering, M., Brinkhuis, H., Damsté, J. S. S., Dickens, G. R., Huber, M., Reichert, G.-J., Stein, R., Matthiessen, J., Lourens, L. J., Pedentchouk, N., Backman, J., Moran, K., and the Expedition 302 Scientists.: Subtropical Arctic Ocean temperatures during the Palaeocene/Eocene Thermal Maximum, *Nature*, 441, 610–613, 2006. 1935, 1943
- 30

**OBGC in the warm  
climate of the Late  
Paleocene**

M. Heinze and T. Ilyina

Title Page

Abstract

Introduction

Conclusions

References

Tables

Figures



Back

Close

Full Screen / Esc

Printer-friendly Version

Interactive Discussion



Takahashi, T., Broecker, W. S., and Langer, S.: Redfield ratio based on chemical data from isopycnal surfaces, *J. Geophys. Res.-Oceans*, 90, 6907–6924, doi:10.1029/JC090iC04p06907, 1985. 1938

5 Takahashi, T., Sutherland, S. C., Wanninkhof, R., Sweeney, C., Feely, R. A., Chipman, D. W., Hales, B., Friederich, G., Chavez, F., Sabine, C., Watson, A., Bakker, D. C., Schuster, U., Metzl, N., Yoshikawa-Inoue, H., Ishii, M., Midorikawa, T., Nojiri, Y., Körtzinger, A., Steinhoff, T., Hoppema, M., Olafsson, J., Arnarson, T. S., Tilbrook, B., Johannessen, T., Olsen, A., Bellerby, R., Wong, C., Delille, B., Bates, N., and de Baar, H. J.: Climatological mean and decadal change in surface ocean  $p\text{CO}_2$ , and net sea-air  $\text{CO}_2$  flux over the global oceans, *Deep-Sea Res. Pt. II*, 56, 554–577, 2009. 1946

10 Thomas, D., Zachos, J., Bralower, T., Thomas, E., and Bohaty, S.: Warming the fuel for the fire: evidence for the thermal dissociation of methane hydrate during the Paleocene-Eocene thermal maximum, *Geology*, 30, 1067–1070, 2002. 1943

15 Tripathi, A. and Elderfield, H.: Deep-Sea Temperature and Circulation Changes at the Paleocene-Eocene Thermal Maximum, *Science*, 308, 1894–1898, doi:10.1126/science.1109202, 2005. 1935, 1944

Tyrrell, T. and Zeebe, R. E.: History of carbonate ion concentration over the last 100 million years, *Geochim. Cosmochim. Acta*, 68, 3521–3530, doi:10.1016/j.gca.2004.02.018, 2004. 1951, 1955

20 Waddell, L. M. and Moore, T. C.: Salinity of the Eocene Arctic Ocean from oxygen isotope analysis of fish bone carbonate, *Paleoceanography*, 23, PA1S12, doi:10.1029/2007PA001451, 2008. 1944

Wanninkhof, R.: Relationship between wind speed and gas exchange over the ocean, *J. Geophys. Res.*, 97, 7373–7382, doi:10.1029/92JC00188, 1992. 1938

25 Weiss, R.: The solubility of nitrogen, oxygen and argon in water and seawater, *Deep-Sea Res.*, 17, 721–735, 1970. 1948

Weiss, R.: Carbon dioxide in water and seawater: the solubility of a non-ideal gas, *Mar. Chem.*, 2, 203–215, 1974. 1938, 1947

30 Wetzel, P., Maier-Reimer, E., Botzet, M., Jungclaus, J., Keenlyside, N., and Latif, M.: Effects of ocean biology on the penetrative radiation in a coupled climate model, *J. Climate*, 19, 3973–3987, 2006. 1945

**OBGC in the warm climate of the Late Paleocene**

M. Heinze and T. Ilyina

[Title Page](#)[Abstract](#)[Introduction](#)[Conclusions](#)[References](#)[Tables](#)[Figures](#)[Back](#)[Close](#)[Full Screen / Esc](#)[Printer-friendly Version](#)[Interactive Discussion](#)

- Winguth, A., Shellito, C., Shields, C., and Winguth, C.: Climate response at the Paleocene-Eocene Thermal Maximum to greenhouse gas forcing – a model study with CCSM3, *J. Climate*, 23, 2562–2584, doi:10.1175/2009JCLI3113.1, 2010. 1935
- Zachos, J. C., Pagani, M., Sloan, L., Thomas, E., and Billups, K.: Trends, rhythms, and aberrations in global climate 65 Ma to present, *Science*, 292, 686–693, 2001. 1935
- Zachos, J. C., Dickens, G. R., and Zeebe, R. E.: An early Cenozoic perspective on greenhouse warming and carbon-cycle dynamics, *Nature*, 451, 279–283, doi:10.1038/nature06588, 2008. 1935
- Zeebe, R. E.: LOSCAR: Long-term Ocean-atmosphere-Sediment CARbon cycle Reservoir Model v2.0.4, *Geosci. Model Dev.*, 5, 149–166, doi:10.5194/gmd-5-149-2012, 2012. 1939, 1954
- Zeebe, R. E. and Zachos, J. C.: Reversed deep-sea carbonate ion basin gradient during Paleocene-Eocene thermal maximum, *Paleoceanography*, 22, PA3201, doi:10.1029/2006PA001395, 2007. 1952
- Zeebe, R. E. and Zachos, J. C.: Long-term legacy of massive carbon input to the Earth system: Anthropocene vs. Eocene, *Philos. T. Roy. Soc. A*, 371, 1471–2962, doi:10.1098/rsta.2012.0006, 2013. 1935, 1936
- Zeebe, R. E., Zachos, J. C., and Dickens, G. R.: Carbon dioxide forcing alone insufficient to explain Palaeocene-Eocene Thermal Maximum warming, *Nat. Geosci.*, 2, 576–580, doi:10.1038/ngeo578, 2009. 1936, 1953, 1956

## OBGC in the warm climate of the Late Paleocene

M. Heinze and T. Ilyina

Title Page

Abstract

Introduction

Conclusions

References

Tables

Figures

⏪

⏩

◀

▶

Back

Close

Full Screen / Esc

Printer-friendly Version

Interactive Discussion

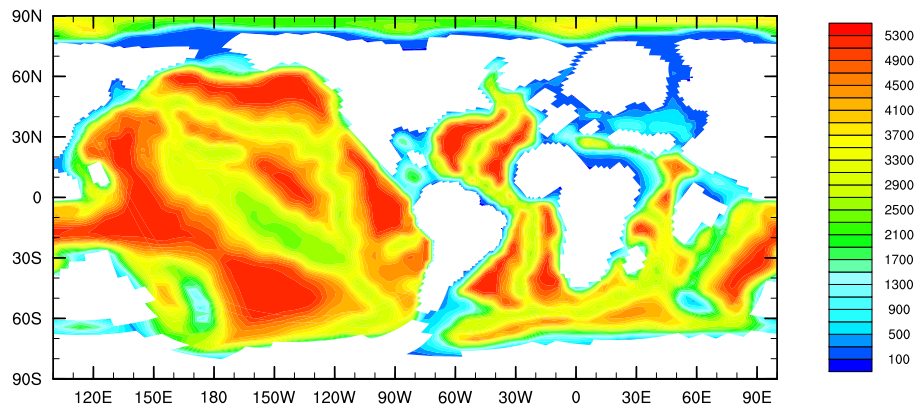


**Table 1.** Model parameters.

Name of Model Parameter/variable	Pre-industrial (CMIP 5)	Late Paleocene
Atmospheric CO <sub>2</sub> (ppm)	278	560
Ocean volume (10 <sup>18</sup> m <sup>3</sup> )	1.353	1.164
Ocean temperature surface (°C)	9.6	24.8
Ocean temperature at 4000 m depth (°C)	1.4	8.9
Ocean salinity	34.67	33.45
<i>Inventories</i>		
Carbon (10 <sup>3</sup> Gt)	38.5	32.0
Phosphate (10 <sup>12</sup> kmol)	2.73	2.48
Silicate (10 <sup>14</sup> kmol)	1.64	1.88
Nitrate (10 <sup>13</sup> kmol)	3.44	2.84
<i>Weathering</i>		
Global input of CaCO <sub>3</sub> (Tmol yr <sup>-1</sup> )	28.4	22.1
Global input of opal (Tmol yr <sup>-1</sup> )	6.5	0
Global input of POC (Tmol yr <sup>-1</sup> )	0	0.1
<i>Primary production</i>		
Global (GtC yr <sup>-1</sup> )	61.14	58.65
<i>Export production</i>		
CaCO <sub>3</sub> (GtC yr <sup>-1</sup> )	0.89	0.63
Opal (Tmol Si yr <sup>-1</sup> )	118.24	159.57
POC (GtC yr <sup>-1</sup> )	8.72	8.54
<i>Molar export ratio</i>		
C(CaCO <sub>3</sub> ) : Si(opal)	0.63	0.33
C(CaCO <sub>3</sub> ) : C(POC)	0.1	0.07
Si(opal) : C(POC)	0.16	0.22

**OBGC in the warm climate of the Late Paleocene**

M. Heinze and T. Ilyina

**Fig. 1.** Paleocene topography (m depth).[Title Page](#)[Abstract](#)[Introduction](#)[Conclusions](#)[References](#)[Tables](#)[Figures](#)[Back](#)[Close](#)[Full Screen / Esc](#)[Printer-friendly Version](#)[Interactive Discussion](#)

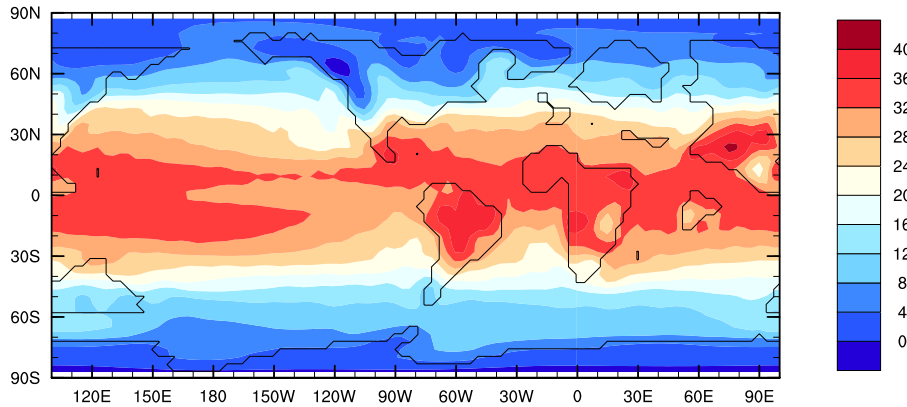


**Fig. 2.** Forcing field: annual mean atmospheric temperature (°C) at 2 m height.

**OBGC in the warm climate of the Late Paleocene**

M. Heinze and T. Ilyina

Title Page

Abstract Introduction

Conclusions References

Tables Figures

⏪ ⏩

◀ ▶

Back Close

Full Screen / Esc

Printer-friendly Version

Interactive Discussion



## OBGC in the warm climate of the Late Paleocene

M. Heinze and T. Ilyina

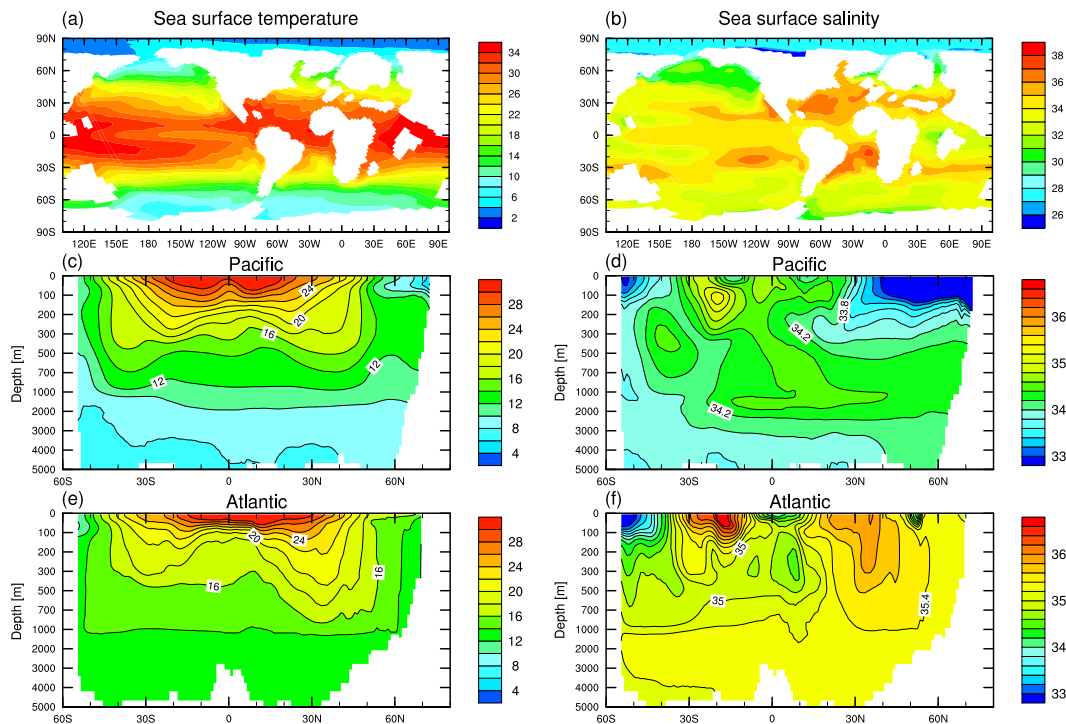


**Fig. 3.** Sea surface temperature ( $^{\circ}\text{C}$ ) (left panels) and salinity (right panels); for the surface (a, b), Pacific (c, d), and Atlantic (e, f) averaged meridional cross cut. Note the non-linear vertical axes, used to zoom in the upper ocean layers.

Title Page

Abstract

Introduction

Conclusions

References

Tables

Figures

◀

▶

◀

▶

Back

Close

Full Screen / Esc

Printer-friendly Version

Interactive Discussion



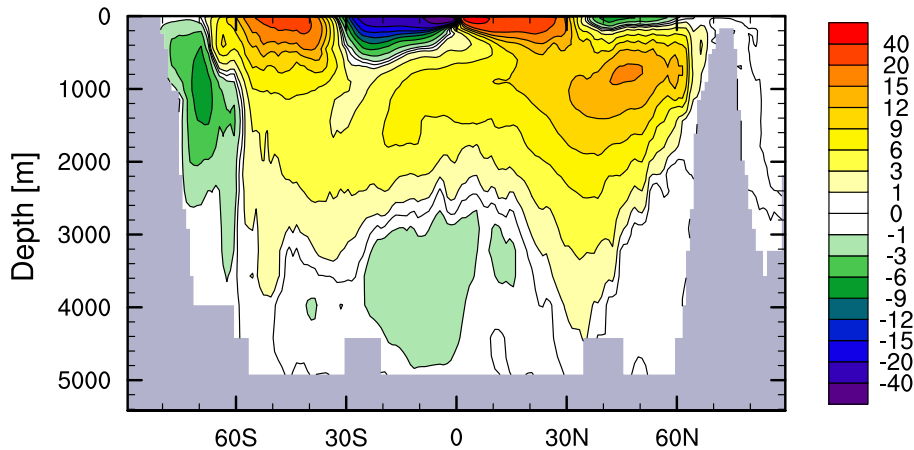


**Fig. 4.** Globally averaged meridional overturning circulation (Sv), positive values correspond to clockwise circulation.

**OBGC in the warm climate of the Late Paleocene**

M. Heinze and T. Ilyina

[Title Page](#)

[Abstract](#)   [Introduction](#)

[Conclusions](#)   [References](#)

[Tables](#)   [Figures](#)

[⏪](#)   [⏩](#)

[◀](#)   [▶](#)

[Back](#)   [Close](#)

[Full Screen / Esc](#)

[Printer-friendly Version](#)

[Interactive Discussion](#)



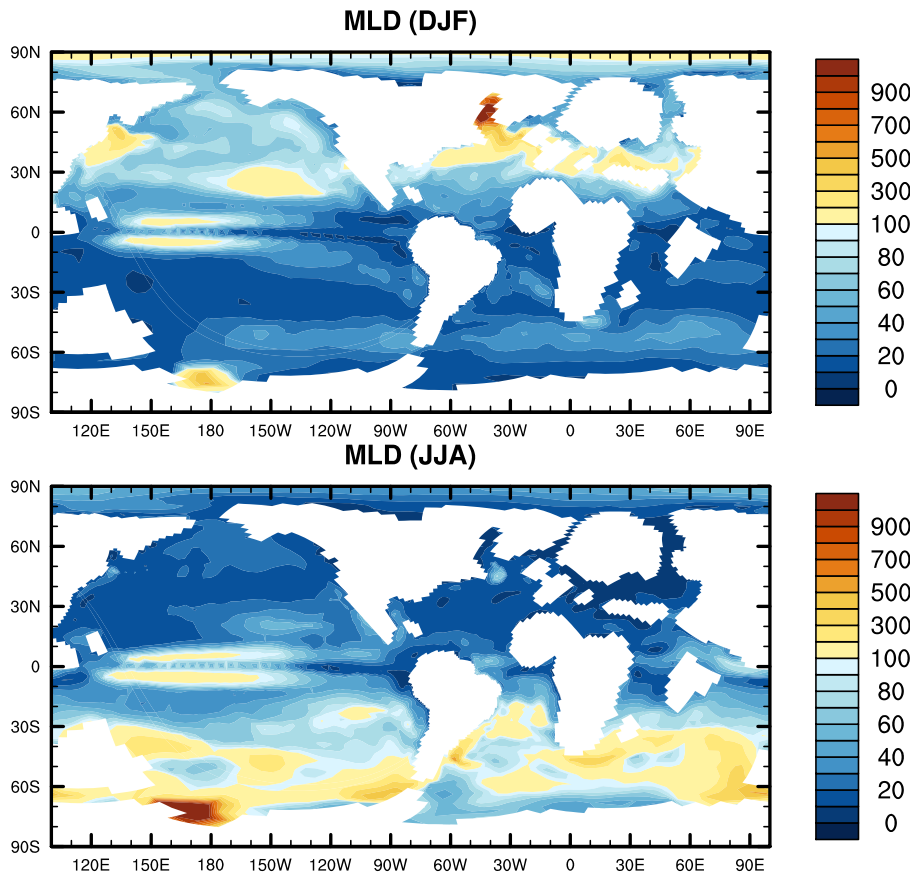


Fig. 5. Mixed Layer Depth (m) averaged over boreal winter (DJF) and boreal summer (JJA).

OBGC in the warm climate of the Late Paleocene

M. Heinze and T. Ilyina

Title Page

Abstract Introduction

Conclusions References

Tables Figures

◀ ▶

◀ ▶

Back Close

Full Screen / Esc

Printer-friendly Version

Interactive Discussion



**OBGC in the warm  
climate of the Late  
Paleocene**

M. Heinze and T. Ilyina

Title Page

Abstract

Introduction

Conclusions

References

Tables

Figures



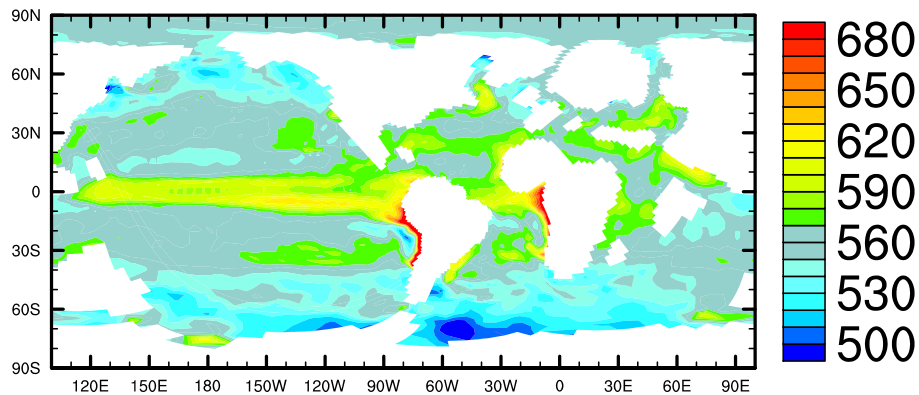
Back

Close

Full Screen / Esc

Printer-friendly Version

Interactive Discussion

**Fig. 6.** Annual mean surface ocean  $p\text{CO}_2$  (ppm).

## OBGC in the warm climate of the Late Paleocene

M. Heinze and T. Ilyina

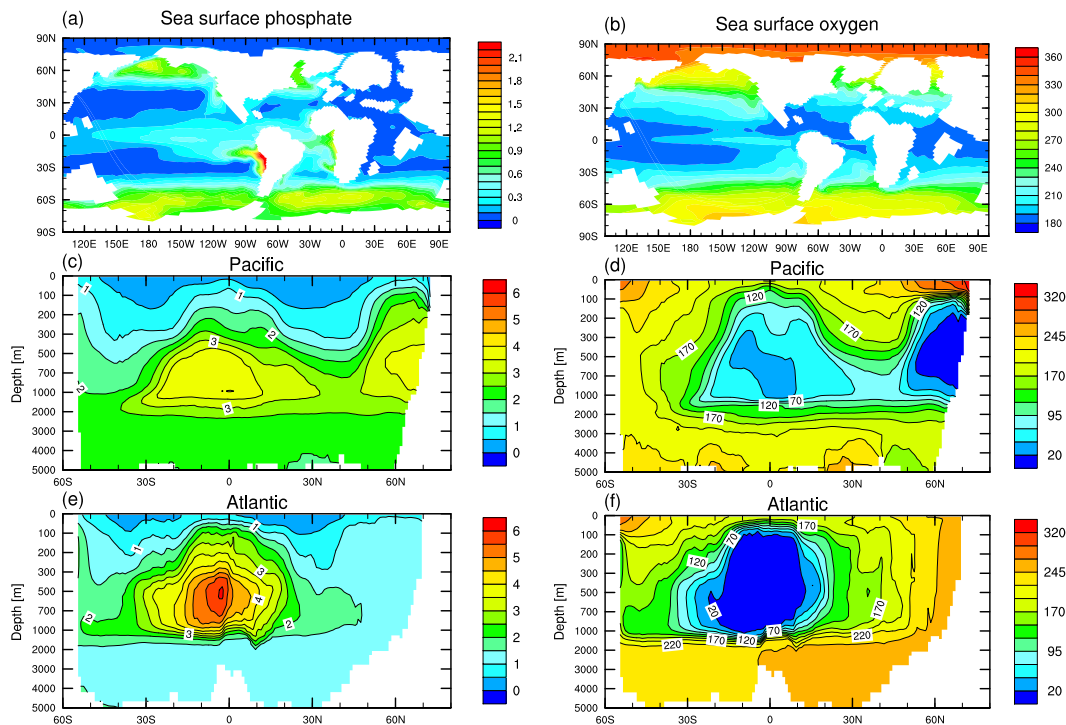


**Fig. 7.** Phosphate (left panels) and oxygen (right panels) concentrations (both in  $\mu\text{mol L}^{-1}$ ); for the surface (**a**, **b**), Pacific (**c**, **d**), and Atlantic (**e**, **f**) averaged meridional crosscut. Note the non-linear vertical axes, used to zoom in the upper ocean layers.

Title Page

Abstract

Introduction

Conclusions

References

Tables

Figures

◀

▶

◀

▶

Back

Close

Full Screen / Esc

Printer-friendly Version

Interactive Discussion



**OBGC in the warm climate of the Late Paleocene**

M. Heinze and T. Ilyina

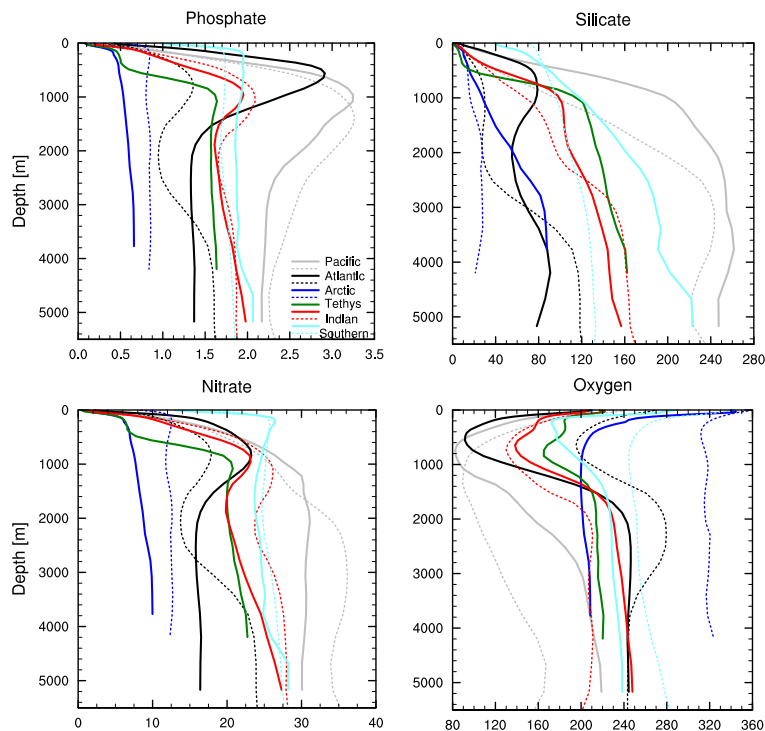


**Fig. 8.** Globally averaged vertical profiles of phosphate, silicate, nitrate and oxygen (all in  $\mu\text{mol L}^{-1}$ ). Solid lines show Late Paleocene distributions, dotted lines show pre-industrial concentrations calculated within CMIP5 experiments.

[Title Page](#)[Abstract](#)[Introduction](#)[Conclusions](#)[References](#)[Tables](#)[Figures](#)[⏪](#)[⏩](#)[◀](#)[▶](#)[Back](#)[Close](#)[Full Screen / Esc](#)[Printer-friendly Version](#)[Interactive Discussion](#)

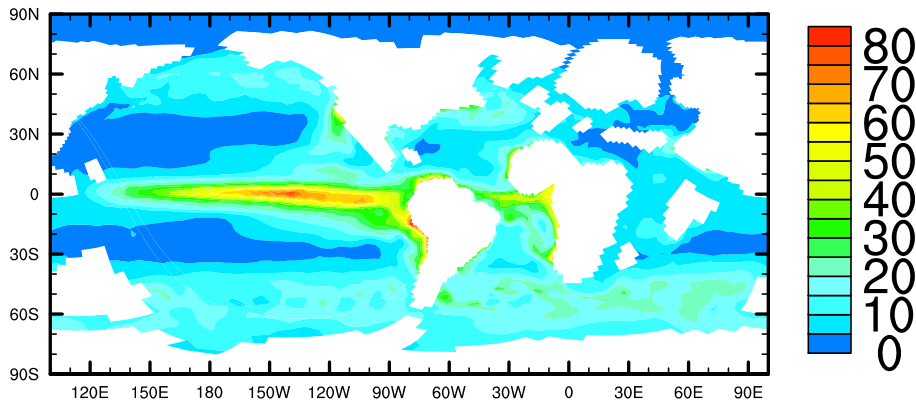


**Fig. 9.** Annual mean primary production ( $\text{mol C m}^{-2} \text{yr}^{-1}$ ).

## CPD

10, 1933–1975, 2014

### OBGC in the warm climate of the Late Paleocene

M. Heinze and T. Ilyina

Title Page

Abstract

Introduction

Conclusions

References

Tables

Figures



Back

Close

Full Screen / Esc

Printer-friendly Version

Interactive Discussion



## OBGC in the warm climate of the Late Paleocene

M. Heinze and T. Ilyina

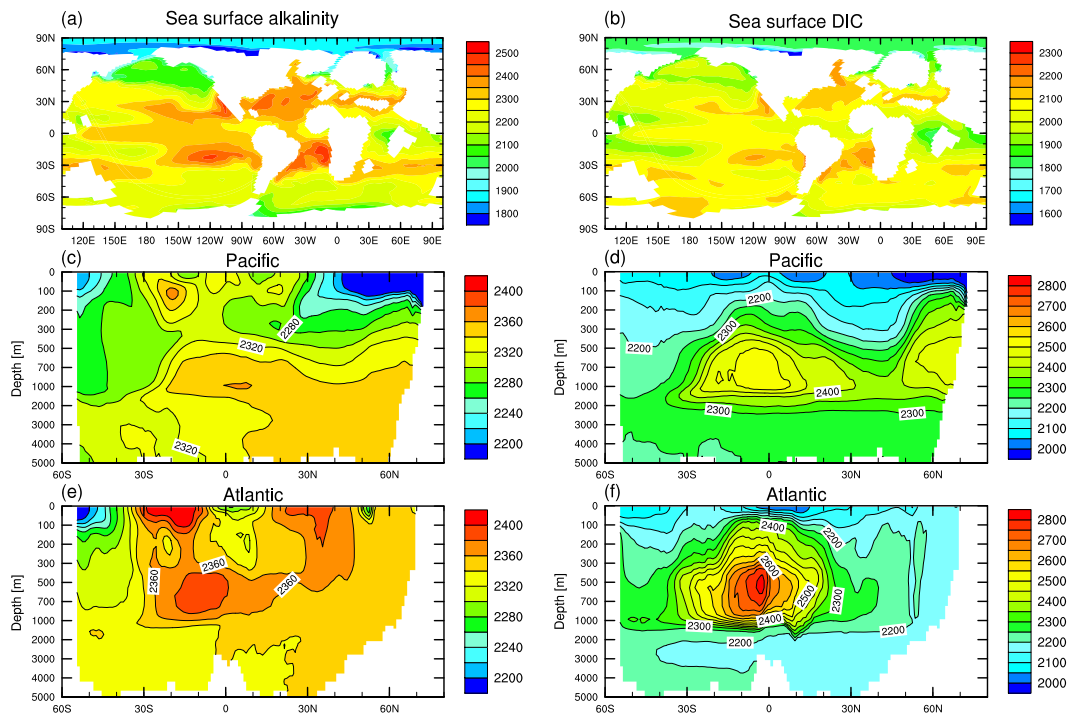


**Fig. 10.** TA (left panels) and DIC (right panels) concentrations (both in  $\mu\text{mol kg}^{-1}$ ); for the surface (a, b), Pacific (c, d), and Atlantic (e, f) averaged meridional crosscut. Note the non-linear vertical axes, used to zoom in the upper ocean layers.

Title Page

Abstract

Introduction

Conclusions

References

Tables

Figures



Back

Close

Full Screen / Esc

Printer-friendly Version

Interactive Discussion

## OBGC in the warm climate of the Late Paleocene

M. Heinze and T. Ilyina

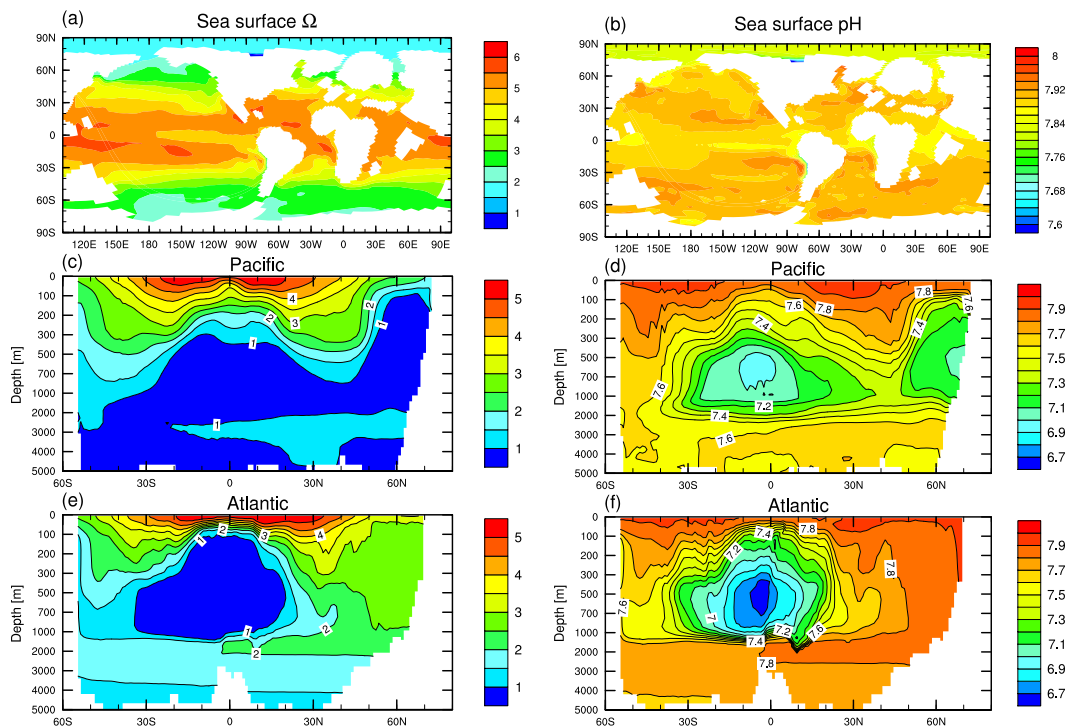


**Fig. 11.**  $\Omega$  (left panels) and pH (right panels); for the surface (a, b), Pacific (c, d), and Atlantic (e, f) averaged meridional crosscut. Note the non-linear vertical axes, used to zoom in the upper ocean layers.

Title Page

Abstract

Introduction

Conclusions

References

Tables

Figures

◀

▶

◀

▶

Back

Close

Full Screen / Esc

Printer-friendly Version

Interactive Discussion



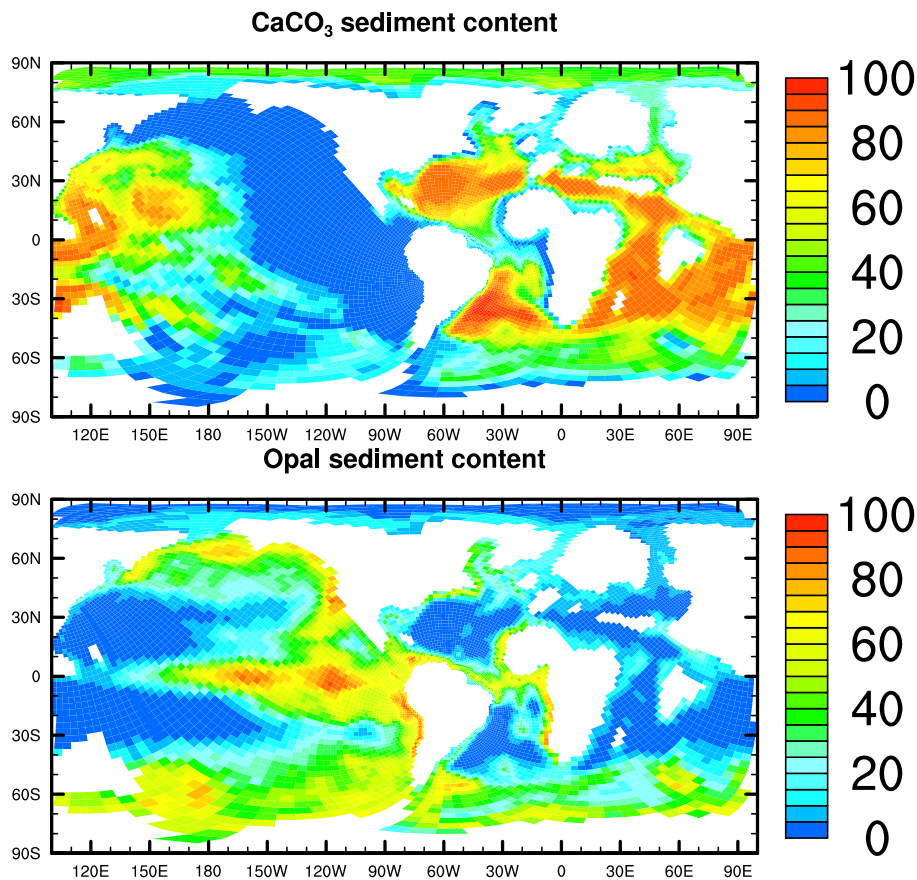


**Fig. 12.** Sediment content of CaCO<sub>3</sub> and opal (both in wt%), averaged over the last 30 years of the simulation.

Title Page

Abstract

Introduction

Conclusions

References

Tables

Figures

⏪

⏩

◀

▶

Back

Close

Full Screen / Esc

Printer-friendly Version

Interactive Discussion

